Appl Phys B (2012) 107:1131–1143
DOI 10.1007/s00340-011-4792-9

Applied Physics B
Lasers and Optics

Electron binding energies from collisional activation of metal-cluster dianions

A. Herlert · L. Schweikhard

Received: 30 April 2011 / Revised version: 15 August 2011 / Published online: 12 November 2011

Abstract Gold-cluster dianions Au_n^{2-}, $n = 21$–31, have been investigated by use of multi-collisional excitation in a Penning trap. At low excitation energies the corresponding singly charged cluster anions have been observed, but no fragments, which indicates the emission of one electron. The binding energy of the surplus electron is deduced from the dianion yield observed as a function of the collision energy by use of a statistical model based on detailed balance. The resulting binding energies of the second electrons are in good agreement with a simple liquid-drop model with empirical corrections including the Coulomb barrier. The double difference of these energies shows a strong odd–even staggering which is compared to the behavior of the electron affinity of neutral gold clusters.

1 Introduction

About 100 years ago, Robert Millikan studied negatively charged oil droplets on the micrometer scale in order to deduce the elementary charge of the electron [1–3] for which he was awarded the Nobel Prize in Physics in 1923. While these droplets contain a large number of atoms and can be treated as small spheres, the question arises: what happens if one goes from the micrometer scale to the nano-scale world with systems of only a few atoms? The special behavior of small molecules and clusters was described with the simple phrase 'Small is different' [4], pointing out the dramatic changes in the physical and chemical properties of small clusters if just one atom or even an electron is added or removed. Several experimental observations have confirmed the presence of the so-called 'magic' cluster sizes resembling closed geometric or electronic shells, which exhibit a higher stability as compared to neighboring cluster sizes [5–13].

With respect to charging clusters or molecules with additional electrons, experimental and theoretical investigations were pursued in order to find the limit of stability for doubly or multiply charged anionic molecules or clusters [14–16]. What could be the smallest molecule with two additional electrons? The existence of these dianions was shown on several occasions, for example for fullerenes [17–20] and small molecules [21–24]. In 1999 the first observation of dianionic metal clusters was reported [25], which was followed by a systematic study of their properties [26–28]. These investigations focused on the production, the onset of formation and relative abundances as a function of the cluster size. The comparison of the experimental results to theoretical predictions was performed in a more qualitative fashion.

Recently, the first results of photoexcitation experiments on gold-cluster dianions were reported including a value for the binding energy of the surplus electron for Au_{29}^{2-} [29] and a first hint to a size-dependent decay branching ratio for monomer evaporation and electron emission [13, 30]. Up to now, no further experimental electron affinities of monoanionic gold clusters Au_n^{1-} are known and only extrapolations from neutral clusters and theoretical values are available [27]. In the present work, a complementary study is presented where size-selected gold-cluster dianions are subjected to multiple collisions with argon atoms in a Pen-

A. Herlert · L. Schweikhard
Institut für Physik, Ernst-Moritz-Arndt-Universität Greifswald, 17487 Greifswald, Germany

Present address:
A. Herlert (✉)
FAIR GmbH, Planckstr. 1, 64291 Darmstadt, Germany
e-mail: a.herlert@gsi.de

ning trap to increase the total energy above the threshold for electron emission. In general, the investigation of stored metal clusters by use of collisions with inert gas atoms provides decay pathways and binding energies deduced from the observed ion yields [31–33].

With the production of multiply negatively charged clusters new charge states are available and therefore changes of the decay pathways are possible, in particular emission of electrons competing with the evaporation of atoms. Furthermore, as shown below, experimental electron affinities can be obtained, which will be compared to predicted values.

2 Liquid-drop-model description

Before reporting on the experimental procedure and data, the liquid-drop model (LDM) of metal clusters, which will be the basis of the discussion of the results, is briefly reviewed. Following the characterization of nuclei by von Weizsäcker [34] metal clusters can be treated with a simple LDM description [35]. In the present work the following parameters and equations will be used. The cluster radius is approximated by

$$R(n) = r_0 n^{1/3}, \tag{1}$$

where n is the number of atoms and $r_0 = 1.59$ Å the Wigner–Seitz radius of gold [36]. The ionization potential (IP), i.e. the energy for removing an electron regardless of the initial charge state, and the electron affinity (EA), i.e. the energy released in the attachment of an electron, are given by [28]

$$\begin{aligned} IP(n, z-1 \to z) &= EA(n, z \to z-1) \\ &= W + \left(z - \frac{1}{2}\right) \frac{1}{4\pi\varepsilon_0} \frac{e^2}{R(n)}, \end{aligned} \tag{2}$$

where $W = 5.38$ eV is the bulk work function of gold (mean value of data given in [37]), z the charge state of the cluster. A possible spill-out of electrons [27] is neglected. In the case of a dianionic gold cluster Au_n^{2-} with $z = -2$, the binding energy of the second surplus electron is equal to the electron affinity of the monoanionic gold cluster Au_n^{1-}:

$$E_B(n) = EA(n, z = -1) = IP(n, z = -2). \tag{3}$$

In addition to the electron affinity, the Coulomb barrier has to be taken into account when determining the detachment energy of the surplus electron (tunneling through the barrier is neglected), i.e. the energy needed to remove one electron from the dianion ($z = -2$). In Fig. 1 the Coulomb barrier is shown for the cluster anion Au_{21}^{1-}. It has been calculated using the classical description of an isolated conducting sphere [38]:

$$V_C(r, R, z) = \frac{e^2}{4\pi\varepsilon_0} \left(\frac{|z|}{r} - \frac{R^3}{2r^2(r^2 - R^2)} \right). \tag{4}$$

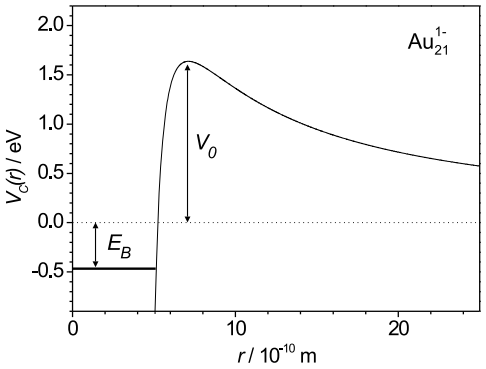

Fig. 1 Coulomb barrier of the gold-cluster monoanion Au_{21}^{1-} as given in (4) with the binding energy E_B of the surplus electron indicated. V_0 is the maximum of the Coulomb barrier (see (5))

For the determination of the binding energy E_B, the Coulomb barrier height for a monoanionic cluster ($z = -1$) is of importance:

$$V_0(R) = \frac{e^2}{8\pi\varepsilon_0 R}, \tag{5}$$

as well as the distance of the maximum from the center of the cluster [26]:

$$R_0(R) = \frac{\sqrt{5}+1}{2} R. \tag{6}$$

On the one hand, the Coulomb barrier impedes the attachment of electrons. On the other hand, it stabilizes multiply charged clusters or molecules, as the additional electron would be emitted immediately in case of a negative electron affinity. For example, the fullerene dianion C_{60}^{2-} was observed up to several seconds [17, 18] although the monoanionic C_{60}^{1-} has a negative electron affinity [39]. In contrast, vibrationally hot C_{60}^{2-} can decay within milliseconds via tunneling of an electron through the Coulomb barrier as reported in [40]. In comparison, vibrationally hot C_{70}^{2-} was observed to be stable for seconds due to its slightly positive electron affinity [40, 41].

In Fig. 2 the relative abundance of gold (filled squares), silver (open circles) and copper (filled triangles) cluster dianions and trianions is plotted as a function of the cluster radius as defined in (1) (data from [28]). The electron affinity has been added to the plot in order to indicate the expected size region of dianion and trianion appearance. Dianions are observed only for sizes somewhat larger than expected from the LDM limit. In the case of trianions, the experimentally observed multiply charged ions appear for sizes significantly smaller than the expected LDM limit, most probably due to the presence of the Coulomb barrier which prevents direct electron emission. Furthermore, for certain cluster sizes either reduced or enhanced production yields are observed which can be related to the (magic) numbers of valence electrons and the corresponding electronic shell closures [26, 27,

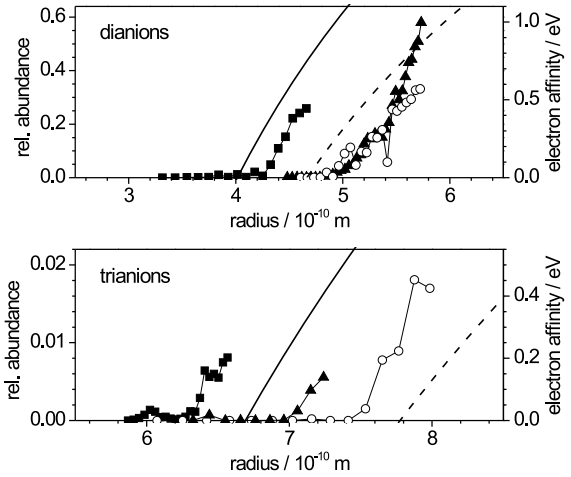

Fig. 2 Relative abundance of dianions (*top*) and trianions (*bottom*) as a function of the cluster size for gold (*filled squares*), silver (*empty circles*), and copper (*filled triangles*). The *solid* and *dashed lines* give the LDM electron affinity for gold and silver/copper cluster monoanions and dianions, respectively. Data taken from [28]

42]. Although these observations can give a qualitative picture and understanding of the onset of creation of dianions and trianions, a more quantitative approach is needed to obtain electron affinities.

An estimate of the expected electron affinity and thus of the electron binding energy can be obtained by use of empirical corrections to the LDM trend. In Fig. 3 (top) experimental values [43] of the electron affinity of neutral gold clusters, Au_n, are shown (filled circles). The solid line gives the LDM behavior as a function of the cluster size. The difference of the experimental and LDM values is shown in Fig. 3 (middle). Besides the odd–even staggering [44] for smaller cluster sizes ($n < 30$), the closed valence-electron shells at $n_e = 34$ and 58 clearly govern the electron affinity. These differences are taken into account for an empirical correction of the electron affinity of monoanionic gold clusters, Au_n^{1-}. The values are added to the LDM electron affinities where the number of valence electrons n_e is matched rather than the cluster size n. The result for $EA(n, z = -1)$ is shown in Fig. 3 (bottom).

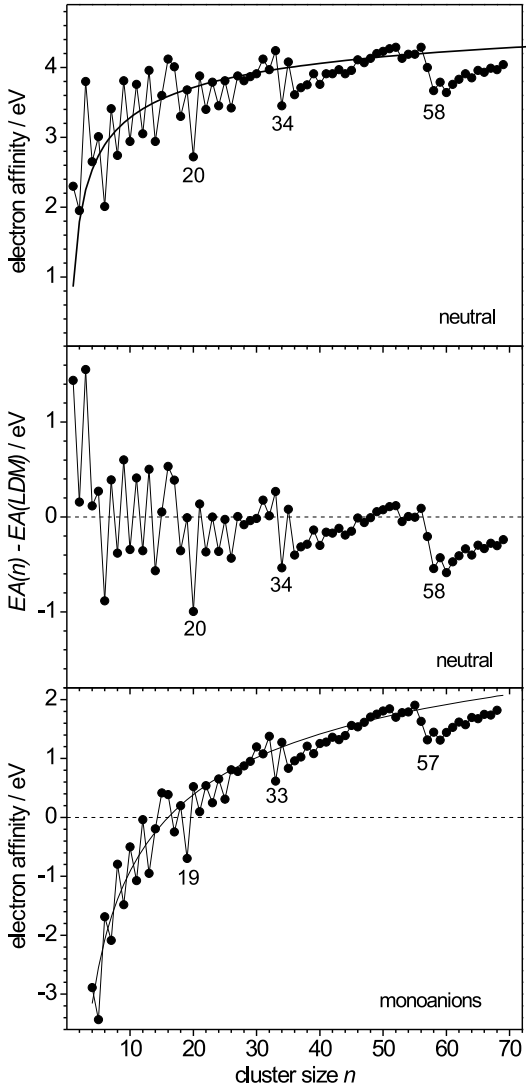

Fig. 3 *Top*: Electron affinity of neutral gold clusters Au_n (*filled circles*, data taken from [43]). The *solid line* is the LDM trend as given in (2) (with parameters for gold given in the text). *Center*: Deviation of the electron affinity from the LDM values. *Bottom*: Electron affinity of monoanions Au_n^{1-} as a function of the cluster size. The data have been deduced from the LDM trend of monoanionic gold clusters (*solid line*) and empirical corrections taken from neutral gold clusters. The *numbers* indicate cluster sizes with closed electronic shells, i.e. number of valence electrons $n_e = 20$, 34, 58

3 Experimental setup and procedure

3.1 Experimental setup

The experiments were carried out at the ClusterTrap experiment [45] which is dedicated to the investigation of size-selected clusters by use of a Penning trap. It consists of a laser-vaporization ion source [46] which creates neutral and singly charged metal clusters. Either the cations or the anions are transferred to the Penning trap, captured in-flight, and accumulated [47]. The hyperbolically shaped Penning trap is used as a container to hold the ions almost at rest for the cluster investigations by various preparation and examination steps. The ions are analyzed by use of an adjacent time-of-flight (ToF) mass spectrometer with single-ion counting capability. The stored cluster ions can interact with photons from a pulsed Nd:YAG or dye laser [48–50], or the cluster ions can be subjected to collisions with inert buffer gas for cooling [47] and collision induced dissociation [31–33]. For the latter, the ring electrode is split in order to allow the application of radiofrequency (rf) excitations of the ion motions. In general, the ions in a Penning trap have three

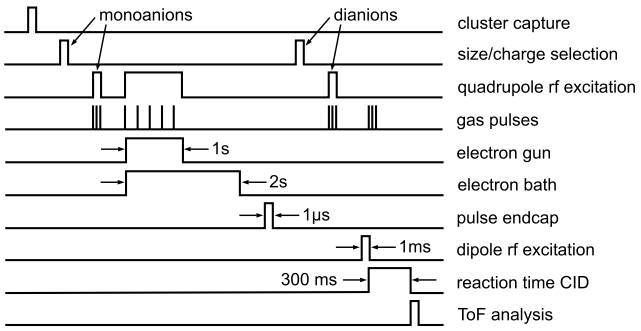

Fig. 4 Schematic experimental cycle of the collision induced dissociation measurements

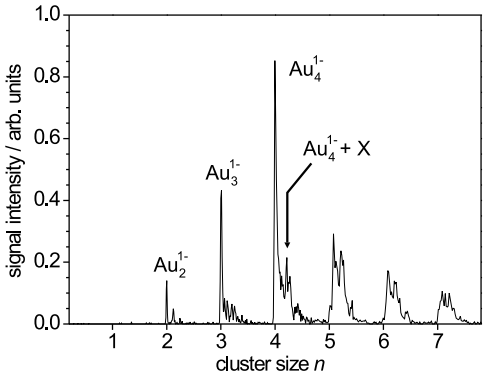

Fig. 5 Mass spectrum of small monoanions Au_n^{1-}, $n = 2$–7, as accumulated in the Penning trap

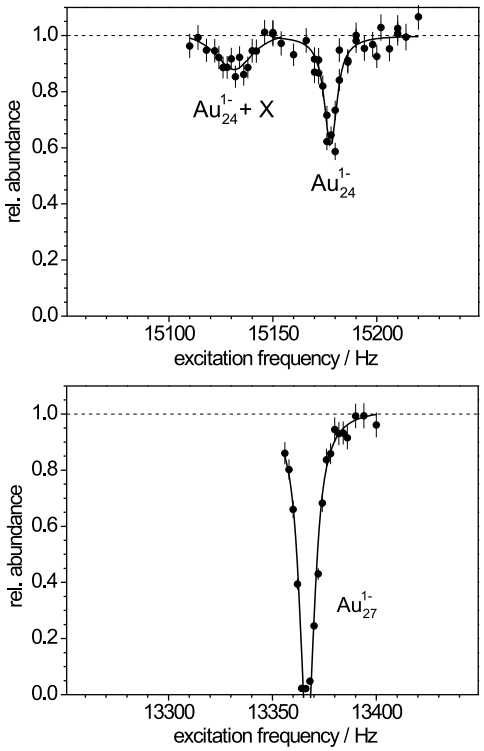

Fig. 6 Relative abundance of monoanions Au_{24}^{1-} (*top*) and Au_{27}^{1-} (*bottom*) after dipolar rf excitation as a function of the excitation frequency. The *solid line* is a Lorentzian fit to the data points to guide the eye

independent motional modes, which are described in detail in [51, 52]. In the following the radial modes are of interest only.

3.2 Experimental cycle

The experimental cycle of the present work is shown in Fig. 4: The singly charged metal clusters are produced in a laser-vaporization source and transferred to the Penning trap. After size selection of the cluster monoanion of interest, an electron beam from an external electron gun is guided through the trap while argon gas is pulsed into the trap volume. The secondary low-energy electrons are simultaneously trapped with and eventually attach to the stored monoanions. Next, the dianions are charge-state selected by removing the monoanions. With a buffer-gas assisted quadrupolar rf excitation [53], the dianions are centered in the trap and thermalized to room temperature before the application of collisional activation by use of a dipolar rf excitation and subsequent buffer-gas pulses. In the following, the various experimental steps are explained in more detail.

3.3 Cluster purification

Since any contamination can lead to deviations of the chemical and physical properties, it is important to select the bare clusters. Thus, in a first step, the clusters are selected by mass separation in the Penning trap. Figure 5 shows a mixture of gold-cluster monoanions as produced in the laser-vaporization source. The abundance of Au_4^{1-} is larger due to multiple ion capture, i.e., accumulation of several ion bunches with subsequent mass-selective buffer-gas cooling [47]. Clearly, the bare gold-cluster anions Au_n^{1-} can be seen. However, admixtures forming molecular ions are present as well. Therefore, the cluster ions are selected by use of the SWIFT technique [54].

In order to cut away unwanted species from the mass spectrum, a dipolar rf excitation is applied to the ring electrodes at two frequency bands corresponding to the reduced cyclotron frequency of the unwanted ions above and below the mass range of the ions of interest. The amplitude is chosen such that the unwanted ions hit the ring electrodes and are thus removed from the trap volume. The cluster selection is defined by the lower and upper limit of the mass range between the two frequency bands, i.e. if properly applied only the bare cluster ions of interest remain in the trap after the SWIFT cleaning.

In order to test the selection procedure and the parameters applied, the high mass selectivity and mass resolution of Penning traps is used. The resolving power is shown in Fig. 6 where the gold-cluster anions Au_{24}^{1-} and Au_{27}^{1-} are examined using a dipolar rf excitation of the cyclotron mo-

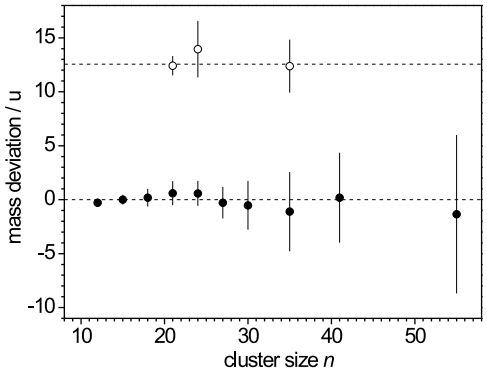

Fig. 7 Deviation from expected mass of bare gold-cluster anions as deduced from the excitation of the cyclotron motion. For details see text

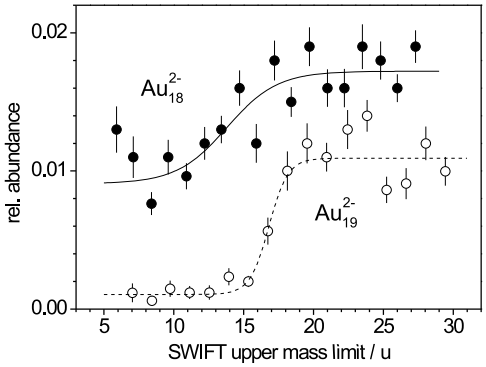

Fig. 8 Relative abundance of dianions Au_{18}^{2-} (*filled circles*) and Au_{19}^{2-} (*empty circles*) as a function of the upper mass limit of the SWIFT mass selection applied to the monoanions in the beginning of the production cycle. The *lines* are drawn to guide the eye

tion followed by ejection of the ions to the ToF mass spectrometer. The excitation amplitude has been chosen to bring the ions to such a large cyclotron radius so that they cannot leave the trap through the ejection bore of the Penning trap and thus do not reach the ion detector. The abundance of ions is then monitored relative to a reference cycle in which no dipolar rf excitation is applied. The resulting relative ion yield is shown in Fig. 6 as a function of the excitation frequency. In the case of Au_{27}^{1-} the relative ion yield goes to zero, i.e. all stored ions are of the same kind. The mass-resolving power is about 1300 ($\Delta\nu \approx 10$ Hz at FWHM) which gives $\Delta m = 4$ u, i.e. only H atoms or H_2 cannot be resolved. As a main contamination atoms or molecules around mass 13 u have been found (see Fig. 6 (top)).

In Fig. 7 the deviation from the expected mass of the bare cluster anions is plotted as a function of the cluster size. Data points with filled circles show the data of clean cluster anions while empty circles give the additional mass with respect to a bare cluster. The upper dashed line gives the average of the three data points. Since the excitation duration was fixed at 100 ms the absolute mass uncertainty increases for larger clusters. Nevertheless, once the SWIFT cleaning has been applied with the proper frequency bands, no contamination is observed.

Figure 8 demonstrates the influence of atoms or molecules attached to the clusters. The relative abundance of gold-cluster dianions Au_{18}^{2-} and Au_{19}^{2-} is plotted as a function of the upper mass limit of the SWIFT mass range of the ions of interest, i.e. for the monoanions Au_{18}^{1-} and Au_{19}^{1-}. Above an additional mass of about $A = 13$, the yield increases, especially in the case of Au_{19}^{2-} which is suppressed for a bare cluster due to the closed electronic shell (valence electrons $n_e = 20$) of Au_{19}^{1-}. With this method the mass resolution is not as high as in the case of the resonant dipolar excitation. However, the attachment of an atom or a molecule in the mass range $A = 13$ fits with the observation made with the dipolar rf excitation. For all measurements shown in the following the SWIFT mass band was chosen to obtain bare gold-cluster anions or dianions.

3.4 Dianion production

The procedure for the attachment of a surplus electron to singly charged and stored cluster ions is described in detail in [28]. In short, the cluster monoanions are superposed with an electron cloud in the Penning trap. The electrons originate from the ionization of argon gas in the trap volume. To this end, an electron beam from an external electron gun ($E = 100$ eV) is guided for one second through the trap. The secondary low-energy electrons can overcome the Coulomb barrier and attach to the singly charged clusters. After switching off the electron beam, the clusters remain for another second in the electron bath to create further dianions. The number of dianions produced depends on the initial number of stored monoanions, the applied trapping potential [55], and the experimental parameters related to the electron bath, e.g. duration and energy of the applied electron beam as well as the amount of argon gas pulsed into the trap volume. All parameters have been chosen such that tens of gold-cluster dianions are available in each experimental cycle.

4 Collisional activation of dianions

The experimental method of collisional activation, i.e. collision induced dissociation (CID), has been described in detail elsewhere (see e.g. [31] and references therein): After size selection and cooling to the center of the trap, the cluster ions are excited with a 1-ms dipolar rf signal, i.e. they are brought to a larger cyclotron radius. This radius is proportional to the excitation amplitude [56] which results from several devices (frequency generator, relays, amplifier, 180° phase shifter) and is monitored at the vacuum feedthrough.

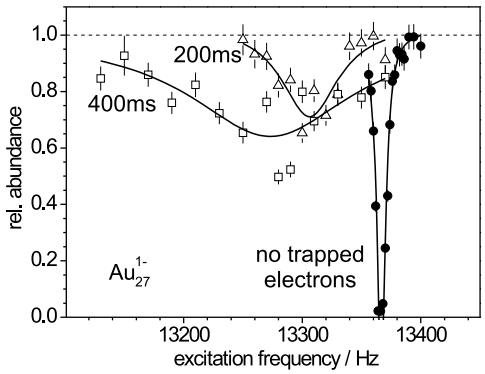

Fig. 9 Relative abundance of monoanions Au_{27}^{1-} after dipolar rf excitation as a function of the excitation frequency. The data series show results after no electron bombardment (*filled circles*), 200 ms (*empty triangles*) and 400 ms (*empty squares*) electron bombardment. The *solid lines* are Lorentzian fits to the data points in order to guide the eye

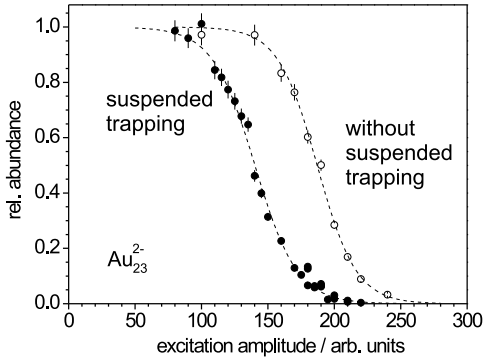

Fig. 10 Relative abundance of dianions Au_{23}^{2-} after dipolar rf excitation as a function of the excitation amplitude (*filled circles* are data taken with suspended trapping, *empty circles* denote data without suspended trapping)

Immediately after the dipolar rf excitation several gas pulses are applied in order to initiate collisions. As the ions collide they lose kinetic energy and are brought back to the center of the trap for ejection and time-of-flight mass spectrometry.

4.1 Space-charge effects

Compared to previous CID investigations at the ClusterTrap setup, the experiments with dianions require some care with respect to the presence of the electron cloud in the trap after electron attachment. In Fig. 9 the relative abundance of monoanions Au_{27}^{1-} after dipolar rf excitation is shown for different space-charge conditions. The rf excitation amplitude has been kept fixed and only the excitation frequency was varied. Clearly, a shift of the resonance frequency can be observed in addition to a broadening of the cyclotron resonance when electrons are present in the trap. That leads to a systematic shift in the collisional-activation experiments if not taken into account. Similar space-charge effects have been observed at other Penning trap experiments [57, 58]. Figure 10 compares a CID result obtained with and without space charge. The electrons can be removed by suspended trapping, i.e., pulsing one endcap electrode for only 1 µs, which allows the electrons to leave the trap, but which is too short to affect the more slowly moving cluster dianions [59].

4.2 Influence of charge-changing reaction

An additional challenge arises in the investigation of dianionic metal clusters using collisional activation. Upon detachment of the surplus electron, the mass-over-charge ratio changes by a factor two and, thus, immediately the ion trajectory changes as discussed in detail in [60]. As a main result, those ions, which are orbiting on a cyclotron radius of one third of the trap radius are at the limit of staying trapped

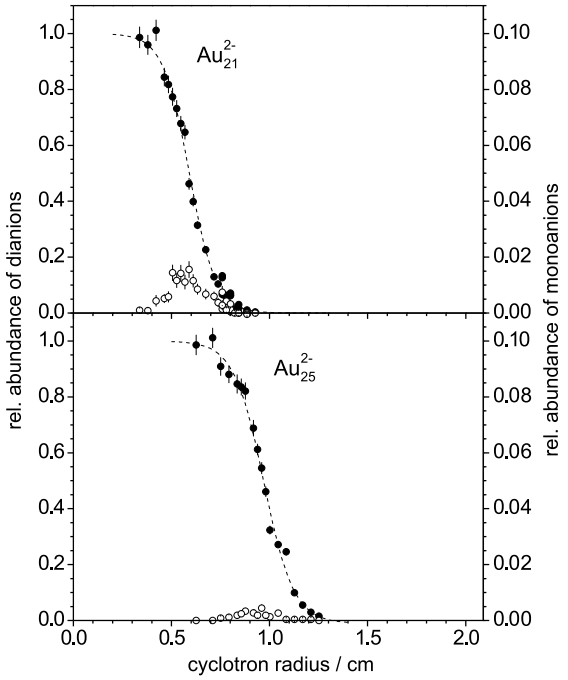

Fig. 11 Relative abundance of dianions Au_n^{2-} (*filled circles*) and monoanions Au_n^{1-} (*empty circles*), $n = 21, 25$, as a function of the initial cyclotron radius after dipolar rf excitation. The scale for the data of monoanions has been increased by a factor 10. The *dashed lines* are drawn to guide the eye

after electron emission. Therefore, the product clusters after electron emission, i.e., the singly charged metal clusters, are not anymore observed for high rf excitation amplitudes. In Fig. 11 results for the collisional activation of dianionic clusters Au_n^{2-}, $n = 21, 25$, are shown. The relative ion abundance is plotted as a function of the cyclotron radius which is reached by the cluster dianions after the dipolar rf excitation. While the relative dianion yield decreases with increasing excitation energy, the product clusters first start to appear as expected, but their yield decreases at a radial distance of

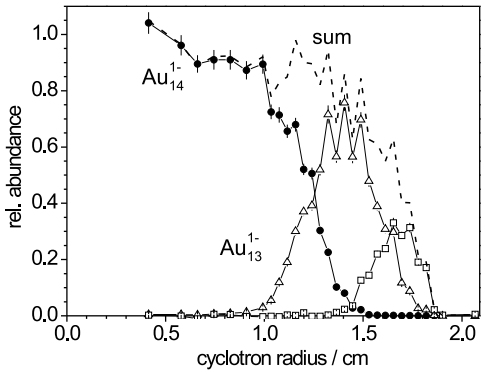

Fig. 12 Relative abundance of Au_{14}^{1-} cluster anions (*filled circles*) and products Au_{13}^{1-} (*empty triangles*) and $Au_{n\leq 12}^{1-}$ (*empty squares*) after collisional activation as a function of the initial cyclotron radius after dipolar rf excitation. The sum of all observed ions is given by the *broken line*

about 0.7 cm. Due to this ion loss, the electron binding energy is determined from the decrease of the dianion yield only.

In order to cross-check the experimental cycle and the conditions, the same experiment was performed for singly charged gold clusters Au_{14}^{1-}. Au_{14}^{1-} has the same mass-over-charge ratio as Au_{28}^{2-} and thus the same cyclotron frequency. Furthermore, Au_{14}^{1-} was recently investigated by use of photoexcitation [61] and thus the data can be applied for the energy calibration (see below). The result is shown in Fig. 12. The number of Au_n^{1-} ions, $n \leq 14$, relative to the number of Au_{14}^{1-} ions in a reference cycle without dipolar rf excitation, is plotted as a function of the cyclotron radius. While the yield of the precursor cluster ions Au_{14}^{1-} decreases, the products Au_{13}^{1-} and smaller cluster anions appear in the mass spectrum for increasing excitation amplitudes. The sum of all ions in the mass spectrum shows a decrease above a cyclotron radius of 1.5 cm which is much larger than the one where the cluster monoanions are lost after electron emission from the doubly charged clusters. This shows the difference between atom evaporation and electron emission with respect to the change of the ion trajectory.

5 Data evaluation

5.1 Impulsive collision theory

Following the work presented in [62, 63] the collisional excitation energy can be estimated in the framework of the *impulsive collision theory* (ICT), where the inelastic collisions of the clusters with the gas atoms are described by elastic collisions of the single cluster-atoms with the gas atoms. For a cluster of total mass $M = nm_A$, which is composed of n atoms with mass m_A each, that collides with a gas atom of mass m_G, the ratio of the energy transfer during the collision, ΔE_{ICT}, to the change of the kinetic energy of the cluster, ΔE_{KIN}, is given by [31]

$$\frac{\Delta E_{\mathrm{ICT}}}{\Delta E_{\mathrm{KIN}}} = \frac{(n-1)m_G}{(n-1)m_G + nm_A}, \tag{7}$$

independent of the scattering angle. In order to obtain sufficient excitation energy to initiate a decay, a single collision is not sufficient. Thus, multi-collisional excitation is required and for each of the single collisions (7) applies. According to this ansatz the total energy transferred to the internal modes of the cluster after many collisions, i.e., when the cluster ion has essentially been stopped by the collision gas, would be

$$E_{\mathrm{ICT}} = \frac{(n-1)m_G}{(n-1)m_G + nm_A} E_{\mathrm{KIN}}. \tag{8}$$

However, the excitation energy is overestimated since the cluster-atoms are not fully free but bound to the cluster. In order to correct the value of the excitation energy an empirical calibration factor C_{MAT} is introduced which depends on the material properties [64]. In addition, for $n > 20$ the ICT model is linearized by taking the limit $n \to \infty$. This results in the collisional excitation energy [31]

$$E_{\mathrm{COLL}} = C_{\mathrm{MAT}} \frac{m_G}{m_G + m_A} E_{\mathrm{KIN}}. \tag{9}$$

The kinetic energy E_{KIN} is determined by the duration (1 ms in the present work) and the amplitude of the dipolar rf excitation of the cyclotron motion (see e.g. [60]). In addition, the initial thermal energy E_{th} ($T \approx 300$ K) has to be taken into account such that the excitation energy E_{EX} reads

$$E_{\mathrm{EX}} = E_{\mathrm{COLL}} + E_{\mathrm{th}}. \tag{10}$$

The emission of an electron or an atom is a statistical process and can be described by a decay rate $k(E_{\mathrm{EX}}, E_B)$, where E_B is the binding energy. The number of precursor clusters N_0 as a function of the excitation energy E_{EX}, normalized to the number of clusters N_A in a reference cycle without excitation, is given by

$$\widetilde{N}_0(E_{\mathrm{EX}}) = \frac{N_0(E_{\mathrm{EX}})}{N_A} = e^{-k(E_{\mathrm{EX}}, E_B)T_R}, \tag{11}$$

where T_R is the reaction duration after the dipolar rf excitation and the subsequent gas collisions, i.e. the experimental period in which the cluster may, e.g., emit an electron or lose an atom. In addition, a Doppler broadening of the excitation energy is assumed due to the thermal distribution of the velocity of the gas atoms relative to the clusters [31]:

$$f_G(\Delta E) = \frac{1}{\sqrt{2\pi}\delta E} e^{-\frac{(\Delta E)^2}{2(\delta E)^2}}, \tag{12}$$

where for simplification a 3σ-area of the Gaussian is considered in the present study. This yields the relative ion abundance as a function of the collisional excitation energy

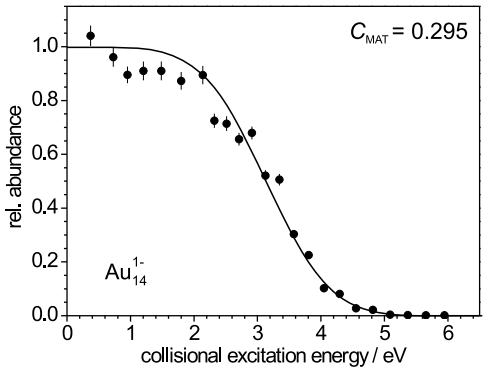

Fig. 13 Relative abundance of Au_{14}^{1-} cluster anions as a function of the collisional excitation energy. The *solid line* is a fit of the expected curve as defined in (13). The calibration factor $C_{MAT} = 0.295$ has been used to match the dissociation energy $D = 2.57$ eV

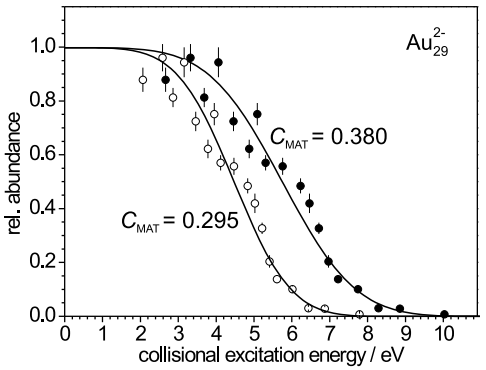

Fig. 14 Relative abundance of Au_{29}^{2-} cluster dianions as a function of the collisional excitation energy. The *solid lines* are fits of the expected curve as defined in (13) for two calibration factors $C_{MAT} = 0.295$ and 0.380. For details see text

E_{COLL}, the binding energy E_B and the Doppler broadening δE:

$$\widetilde{N}_0(E_{COLL}, E_B, \delta E) = \int_{E_{COLL}-3\delta E}^{E_{COLL}+3\delta E} e^{-k(E'+E_{th},E_B)T_R} \times f_G(E' - E_{COLL})\, dE'. \quad (13)$$

5.2 Decay-rate model

The binding energy is implemented in the decay rate of the thermal electron emission, i.e. it is deduced by fitting (13) to the experimental data points. The Weisskopf formalism (see [29] and references therein) predicts a decay rate

$$k(E, E_B) = \frac{2mR_0^2}{\pi\hbar^3}(k_B T_M)^2 \times \exp\{S(E - E_B - V_0) - S(E)\}, \quad (14)$$

where m is the electron mass, R_0 the distance of the maximum of the Coulomb barrier to the center of the cluster, V_0 the Coulomb barrier height, and k_B the Boltzmann constant. $T_M = T(E - E_B - V_0)$ is the temperature of the monoanionic product cluster. The entropy is given by

$$S(E) = \int_0^E dE' \frac{1}{k_B T(E')}. \quad (15)$$

The temperature of the cluster $T(E)$ can be deduced from the energy of the cluster $E(T)$ which is determined using the heat capacity $C_p(T)$ as described in [61]. The energy per atom is

$$E(T) = n_{eff} \int_0^T C_p(T')\, dT', \quad (16)$$

where $n_{eff} = (3n - 6)/3 = n - 2$ is the effective number of atoms (without the translational and rotational modes of the whole cluster). The temperature can be determined by inversion of (16) with the approximation

$$E(T) \approx n_{eff}(a_0 + a_1 T + a_2 T^2), \quad (17)$$

with $a_0 = -16.1$ meV, $a_1 = 0.257$ meV K^{-1} and $a_2 = 1.51 \times 10^{-5}$ meV K^{-2} as given in [29]. Thus the temperature $T(E)$ and the entropy $S(E)$ can be calculated if the energy of the cluster is known.

5.3 Energy calibration

The dissociation of Au_{14}^{1-} is taken for the calibration of the multi-collisional excitation. The ion yield as given in (13) is fitted to the observed relative ion yield shown in Fig. 13 (solid line). The decay rate for atom evaporation is taken from [61]. The calibration factor C_{MAT} is varied until the reduced chi square is minimized for a given dissociation energy $D = 2.57$ eV as known from photoexcitation measurements on Au_{14}^{1-} [61]. This yields a calibration factor $C_{MAT} = 0.295$ which is smaller than the one found for CID measurements on gold-cluster cations ($C_{MAT} = 0.422$, see [32]).

In order to have a second calibration, the recently measured electron binding energy of Au_{29}^{2-} is taken into account, which was obtained by use of time-resolved photoexcitation ($E_B = 0.91(5)$ eV, see [29]). Similar to the calibration in the case of Au_{14}^{1-}, the relative ion yield curve is fitted to the Au_{29}^{2-} data and the parameter E_B is varied to match the expected electron binding energy. A calibration factor $C_{MAT} = 0.380$ is deduced, which is close to the value used in [32]. In Fig. 14 the relative ion yield of Au_{29}^{2-} is plotted as a function of the collisional excitation energy for both calibration factors. For the analysis of all data obtained in this work, both $C_{MAT} = 0.295$ and 0.380 will be applied to calibrate the energy scale.

6 Results

The gold-cluster dianions Au_n^{2-}, $n = 21$–31, have been investigated with collisional activation as described above. In

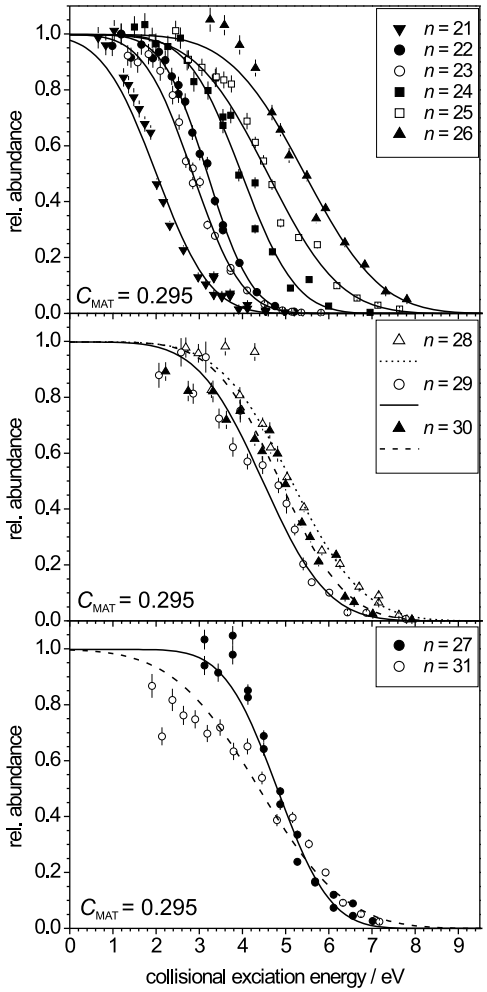

Fig. 15 Relative abundance of dianions Au_n^{2-}, $n = 21$–31, as a function of the collisional excitation energy. The *lines* are fits of (13) to the data. The energy scale has been calibrated with the factor $C_{MAT} = 0.295$

order to avoid the competition with monomer evaporation, the size range has been limited to cluster sizes below $n = 32$ as photoexcitation measurements [13, 30] have shown for Au_{30}^{2-} a ratio between fragmentation and electron emission of about 3%, i.e. reasonably small. At the other end the production yield of Au_{20}^{2-} and smaller gold-cluster dianions was not sufficient for further studies. The fitted curves of the remaining dianions as a function of collisional excitation energy are plotted in Fig. 15 for the calibration factor $C_{MAT} = 0.295$ for cluster dianions Au_n^{2-}, $n = 21$–31. The resulting binding energies for both calibration factors are listed in Table 1.

7 Discussion

The binding energy of the surplus electron for the gold-cluster dianions Au_n^{2-}, $n = 21$–31 is plotted in Fig. 16. The

Table 1 Fit parameters as obtained from data measured in the collisional activation of gold-cluster dianions Au_n^{2-}, $n = 21$–31 for the calibration factors $C_{MAT} = 0.295$ and 0.380. The uncertainties for E_B and δE are $\sigma(E_B) = 0.02$ eV and $\sigma(\delta E) = 0.03$ eV, respectively. The Coulomb barrier height V_0 has been calculated using (5). The last column gives the reduced χ^2 of the fit to the data

		$C_{MAT} = 0.295$		$C_{MAT} = 0.380$		
n	V_0	E_B	δE	E_B	δE	χ_ν^2
21	1.64	−0.27	0.98	−0.03	1.26	10.0
22	1.61	0.19	0.80	0.54	1.04	0.83
23	1.59	0.05	0.89	0.36	1.14	2.31
24	1.57	0.45	0.97	0.87	1.24	10.4
25	1.55	0.64	1.30	1.10	1.67	5.03
26	1.53	0.90	1.36	1.43	1.74	6.15
27	1.51	0.66	0.94	1.11	1.21	17.9
28	1.49	0.74	1.29	1.21	1.66	8.45
29	1.47	0.51	1.16	0.90	1.51	5.86
30	1.45	0.61	1.18	1.03	1.52	8.75
31	1.44	0.45	1.56	0.82	2.00	11.1

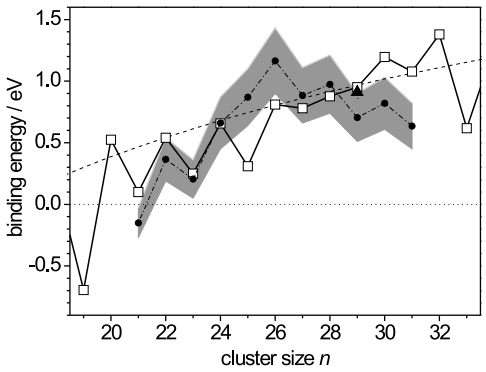

Fig. 16 Binding energy of the surplus electron of the dianions Au_n^{2-}, $n = 21$–31, as a function of the cluster size. The *gray-shaded area* gives the range of experimental values from this work limited by the two calibration factors $C_{MAT} = 0.295$ and 0.380 (the mean value is given by *filled circles*). The *empty squares* give the values deduced from an empirical correction of the LDM values. The *dashed line* gives the LDM trend. The *filled triangle* shows the experimental value from photoexcitation experiments

gray-shaded area shows the range of binding energies with the minimum and maximum values defined by the two calibration factors $C_{MAT} = 0.295$ and 0.380. These experimental values are compared to the LDM trend (dashed line) and to the electron affinity as deduced from the LDM electron affinity of monoanions with empirical corrections (empty squares).

The values from this work show a characteristic odd–even staggering with an increase of the binding energy reaching a maximum at $n = 26$. In general, there is agreement with the LDM behavior (dashed line) and the overlap with the empirically corrected electron affinity (empty

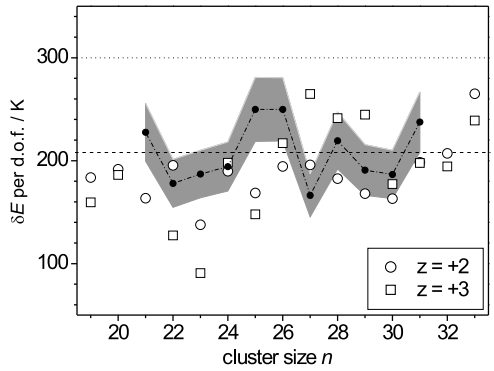

Fig. 17 Energy variation δE (given as temperature) for the dianions Au_n^{2-}, $n = 21$–31, as a function of the cluster size and normalized to the number of degrees of freedom $3n - 6$. The *gray-shaded area* gives the range limited by the two calibration factors $C_{MAT} = 0.295$ and 0.380 (the mean value is given with *filled circles*). The *empty circles* and *squares* give the δE values from the investigation of double and triply charged gold-cluster cations [32]. The *dashed line* shows the mean value of the present fit values δE. The *dotted line* gives the room temperature value

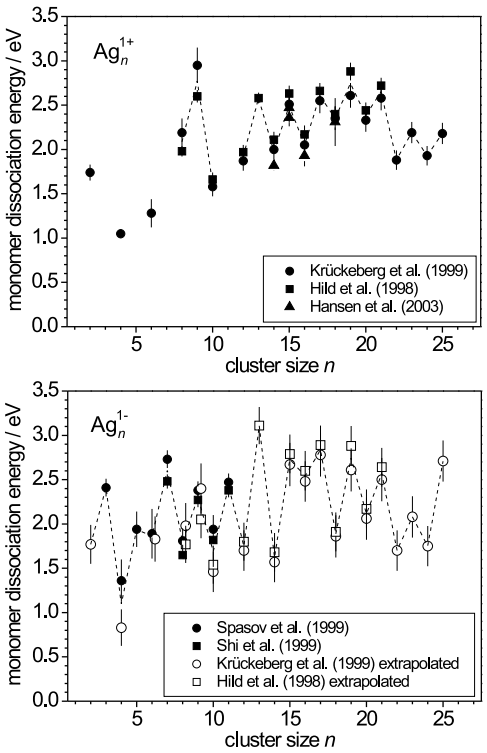

Fig. 18 *Top*: Dissociation energies of silver cluster cations as deduced from time-resolved photofragmentation [49, 65] and CID [31]. *Bottom*: Dissociation energies of silver cluster anions as deduced from time-resolved photofragmentation [66] and CID [67] (*filled symbols*). The dissociation energies indicated by the *empty symbols* are extrapolated from the corresponding data in the *top panel* using (19)

squares) is also good. However, above $n = 26$ the electron affinity is expected to increase while the experimental values tend to decrease slightly and in the case of $n = 25$ a large deviation can be noted, which leads to a smoothing of the odd–even staggering around $n = 25$. This deviation from the empirically corrected LDM values most probably shows a difference of the electron affinities for neutral and monoanionic gold clusters rather than an experimental outlier. Similarly, in the case of neutral gold clusters, a disappearance of the odd–even staggering is observed around $n = 29$ (see Fig. 3), which is not related to a major electronic shell.

In addition to the uncertainty of the calibration factor C_{MAT}, another source of systematic deviation of the binding energy could be a wrong calibration of the amplitude of the dipolar rf excitation which defines the kinetic energy prior to ion-atom collisions. However, such a deviation is expected to be small, especially with respect to the uncertainty imposed by the calibration factor.

Besides the electron binding energy, the only other fit parameter is the Doppler broadening with respect to the gas atoms, represented by the standard deviation δE of the Gaussian distribution. In order to compare the δE values of Table 1, the energy was related to the cluster size by normalizing to the respective degrees of freedom, $3n - 6$. Since this value can be related to a temperature, it has been plotted in Fig. 17 as a function of the cluster size. The shaded area gives the range of values with the boundary defined by the two calibration factors C_{MAT}. The mean value is shown as a dashed line, which is at about 2/3 of the room temperature $T = 300$ K. The normalized fit values fluctuate around the mean value similar to fit values δE from the analysis of CID on multiply charged gold-cluster cations [32] (empty circles and squares in Fig. 17). Thus, the initial cooling and the experimental conditions are comparable. The mean value lower than room temperature can be due to the applied degrees of freedom $(3n - 6)$, which is somewhat an idealized figure and could be different due to the actual cluster structure and couplings. Further investigation of this deviation is required.

The applicability of collisional activation will be assessed by a comparison of dissociation energies obtained with CID and photoexcitation measurements. In the latter case the excitation energy is well defined by the number of absorbed photons plus the initial thermal energy. For singly charged silver cluster cations and anions several experimental values are available and allow a quantitative comparison. In Fig. 18 the values are summarized where the dashed line connects the average values of neighboring cluster sizes. The empty circles in the bottom plot give the extrapolated dissociation energies as calculated with a Born–Haber cycle (see e.g. [61]),

$$\begin{array}{ccccc} X_n^- & \xrightarrow{EA_n} & X_n & \xrightarrow{IP_n} & X_n^+ \\ \downarrow D_n^- & & \downarrow D_n & & \downarrow D_n^+ \\ X_{n-1}^- + X & \xrightarrow{EA_{n-1}} & X_{n-1} + X & \xrightarrow{IP_{n-1}} & X_{n-1}^+ + X \end{array} , \qquad (18)$$

i.e. by taking into account the experimental values for electron affinities EA_n [43] and ionization potentials IP_n [68, 69]

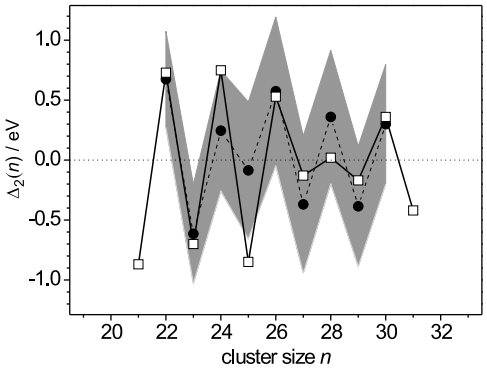

Fig. 19 Double energy difference $\Delta_2(n)$ for Au_n^{2-} as a function of the cluster size n. The *gray-shaded area* gives the experimental values limited by the two calibration factors $C_{MAT} = 0.295$ and 0.380. The *filled circles* are the mean experimental values. The *open squares* are the $\Delta_2(n)$ values obtained from the empirically corrected electron affinities as shown in Fig. 16

of neutral silver clusters of size n to deduce the dissociation energy for the anionic silver clusters:

$$D_n^- = EA_n - EA_{n-1} + IP_n - IP_{n-1} + D_n^+. \quad (19)$$

Overall, the experimental results obtained with CID and photoexcitation are in good agreement. We note that for the cationic silver clusters the photoexcitation data of Ag_n^+, $n = 12, 21$, have been used to calibrate the energy scale for the CID measurements shown in Fig. 18 (top). In particular, the extrapolated data (Fig. 18 (bottom), empty symbols) agree very well with the experimental dissociation energies of the silver cluster anions (filled symbols), which is also a mutual confirmation of the dissociation energies by experiments from two different groups.

In order to compare the relative change in the binding energy of the gold-cluster dianions rather than absolute values, the double difference [70]

$$\Delta_2(n) = 2E_B(n) - E_B(n-1) - E_B(n+1), \quad (20)$$

from the binding energy E_B of Table 1 is plotted in Fig. 19 as a function of the cluster size. The odd–even staggering is well described with a larger deviation for $n = 25$. Neither the cluster size $n = 25$ nor the number of valence electrons $n_e = 27$ has so far been reported to be special with respect to higher stability of gold clusters.

One unknown factor is the Coulomb barrier height V_0, which was taken from the spherical LDM model and fed into the analysis as a fixed parameter for each cluster size. For a better understanding, the actual Coulomb barrier height has to be known. However, the probing of the Coulomb barrier is difficult since it requires a systematic study of the tunneling properties as a function of the temperature of the cluster and thus of the excitation energy of the dianion. Up to now such experimental studies have been reported on fullerenes and small molecules only [71–74].

Furthermore, decay branching, i.e., competing decay pathways cannot be ruled out. From photoexcitation experiments [13, 30] it can be suspected that the ratio between monomer evaporation and electron emission is sufficiently small for the sizes studied here. The decrease of the deduced binding energies for $n > 26$ could be due to a decay-pathway fraction of monomer evaporation larger than expected. However, no doubly charged product clusters were observed which would indicate a significant branching ratio. Additional data from photoexcitation measurements would be beneficial in order to cross-check the observed trend.

8 Conclusion

Size-selected gold-cluster dianions have been studied by use of collisional activation in a Penning trap. For the cluster sizes $n = 21$–31 the binding energy of the surplus electron has been deduced by fitting the expected relative number of surviving dianions to the measured data points. The deduced values were compared to the LDM trend and empirically corrected LDM values. Overall, a good agreement with the LDM behavior is found. However, deviations of the electron affinity of monoanionic gold clusters, especially for Au_{25}^{1-}, with respect to the trend and odd–even staggering of neutral gold clusters are also present which call for further investigation.

Although the Penning trap-based collisional-activation technique is limited due to the fact that the electron emission from Au_n^{2-} leads to the loss of the product cluster Au_n^{1-}, the data obtained give valuable information. Nevertheless, further studies using photoexcitation are required similar to the experiment on Au_{29}^{2-} [29] in order to obtain a better calibration of the energy scale (calibration factor C_{MAT}) and to reduce the uncertainty of the experimental values.

Since the gold clusters are rather heavy in mass, it is difficult to extend the collisional activation to larger clusters. By use of a heavier buffer gas, e.g. krypton or xenon, more energy could be transferred in each collision. Furthermore, the kinetic energy which can be given to the stored clusters is limited due to the Penning trap parameters. It is thus planned to use a 12-T superconducting magnet which will increase the cyclotron frequencies by a factor 2.4 and thus the range of possible kinetic energies by almost a factor 6. It is also envisaged to extend the investigation with collisional activation to silver and copper dianions or other dianionic systems. However, the appearance size of these dianions is larger than in the case of gold-cluster dianions. With the larger number of degrees of freedom the excitation of the dianions above the decay threshold will be challenging.

Acknowledgements This work has been supported by the European Union within the "Cluster cooling" network under contract no. IHP-CT-2000-00026, the Deutsche Forschungsgemeinschaft (DFG) under contract no. SCH401/13-3, and the DFG Collaborative Research Center SFB 652, project A3.

References

1. R.A. Millikan, Philos. Mag. **19**, 209 (1910)
2. R.A. Millikan, Phys. Rev. **32**, 349 (1911)
3. R.A. Millikan, Phys. Rev. **2**, 109 (1913)
4. U. Landman, R.B. Barnett, C.L. Cleveland, H.-P. Cheng, Int. J. Mod. Phys. B **6**, 3623 (1992)
5. O. Echt, K. Sattler, E. Recknagel, Phys. Rev. Lett. **47**, 1121 (1981)
6. W.D. Knight, K. Clemenger, W.A. de Heer, W.A. Saunders, M.Y. Chou, M.L. Cohen, Phys. Rev. Lett. **52**, 2141 (1984)
7. I. Katakuse, T. Ichihara, Y. Fujita, T. Matsuo, T. Sakurai, H. Matsuda, Int. J. Mass Spectrom. Ion Process. **67**, 229 (1985)
8. I. Katakuse, T. Ichihara, Y. Fujita, T. Matsuo, T. Sakurai, H. Matsuda, Int. J. Mass Spectrom. Ion Process. **74**, 33 (1986)
9. A. Selinger, P. Schnabel, W. Wiese, M.P. Irion, Ber. Bunsenges. Phys. Chem. **94**, 1278 (1990)
10. I. Rabin, C. Jackschath, W. Schulze, Z. Phys. D **19**, 153 (1991)
11. S. Krückeberg, G. Dietrich, K. Lützenkirchen, L. Schweikhard, C. Walther, J. Ziegler, Eur. Phys. J. D **9**, 169 (1999)
12. A. Herlert, S. Krückeberg, L. Schweikhard, M. Vogel, C. Walther, J. Electron Spectrosc. Relat. Phenom. **106**, 179 (2000)
13. L. Schweikhard, K. Hansen, A. Herlert, M.D. Herráiz Lablanca, G. Marx, M. Vogel, Hyperfine Interact. **146–147**, 275 (2003)
14. C. Yannouleas, U. Landman, Chem. Phys. Lett. **210**, 437 (1993)
15. M.K. Scheller, R.C. Compton, L.S. Cederbaum, Science **270**, 1160 (1995)
16. A. Dreuw, L.S. Cederbaum, Chem. Rev. **102**, 181 (2002)
17. R.L. Hettich, R.N. Compton, R.H. Ritchie, Phys. Rev. Lett. **67**, 1242 (1991)
18. P.A. Limbach, L. Schweikhard, K.A. Cowen, M.T. McDermott, A.G. Marshall, J.V. Coe, J. Am. Chem. Soc. **113**, 6795 (1991)
19. R.N. Compton, A.A. Tuinman, C.E. Klots, M.R. Pederson, D.C. Patton, Phys. Rev. Lett. **78**, 4367 (1997)
20. O. Hampe, M. Neumaier, M.N. Blom, M.M. Kappes, Chem. Phys. Lett. **354**, 303 (2002)
21. R. Middleton, J. Klein, Phys. Rev. A **60**, 3515 (1999)
22. C.-F. Ding, X.-B. Wang, L.-S. Wang, J. Chem. Phys. **110**, 3635 (1999)
23. X.-B. Wang, L.-S. Wang, Phys. Rev. Lett. **83**, 3402 (1999)
24. J. Friedrich, P. Weis, J. Kaller, R.L. Whetten, M.M. Kappes, Eur. Phys. J. D **9**, 269 (1999)
25. A. Herlert, S. Krückeberg, L. Schweikhard, M. Vogel, C. Walther, Phys. Scr. T **80**, 200 (1999)
26. L. Schweikhard, A. Herlert, S. Krückeberg, M. Vogel, C. Walther, Philos. Mag., B **79**, 1343 (1999)
27. C. Yannouleas, U. Landman, A. Herlert, L. Schweikhard, Phys. Rev. Lett. **86**, 2996 (2001)
28. A. Herlert, L. Schweikhard, Int. J. Mass Spectrom. **229**, 19 (2003)
29. A. Herlert, L. Schweikhard, Int. J. Mass Spectrom. **252**, 151 (2006)
30. L. Schweikhard, K. Hansen, A. Herlert, M.D. Herráiz Lablanca, G. Marx, M. Vogel, Int. J. Mass Spectrom. **219**, 363 (2002)
31. S. Krückeberg, G. Dietrich, K. Lützenkirchen, L. Schweikhard, C. Walther, J. Ziegler, J. Chem. Phys. **110**, 7216 (1999)
32. J. Ziegler, G. Dietrich, S. Krückeberg, K. Lützenkirchen, L. Schweikhard, C. Walther, Int. J. Mass Spectrom. **202**, 47 (2000)
33. S. Krückeberg, L. Schweikhard, J. Ziegler, G. Dietrich, K. Lützenkirchen, C. Walther, J. Chem. Phys. **114**, 2955 (2001)
34. C.F. von Weizsäcker, Z. Phys. **96**, 431 (1935)
35. M. Seidl, M. Brack, Ann. Phys. **245**, 275 (1996)
36. *Handbook of Chemistry and Physics*, 71st edn., ed. by D.R. Lide (CRC Press, Boca Raton, 1990)
37. *Handbook of Chemistry and Physics*, 74th edn., ed. by D.R. Lide (CRC Press, Boca Raton, 1993), pp. 12–105
38. J.D. Jackson, *Classical Electrodynamics*, 2nd edn. (Wiley, New York, 1975), pp. 58–60
39. C. Yannouleas, U. Landman, Chem. Phys. Lett. **217**, 175 (1994)
40. S. Tomita, J.U. Andersen, H. Cederquist, B. Concina, O. Echt, J.S. Forster, K. Hansen, B.A. Huber, P. Hvelplund, J. Jensen, B. Liu, B. Manil, L. Maunoury, S. Brøndsted Nielsen, J. Rangama, H.T. Schmidt, H. Zettergren, J. Chem. Phys. **124**, 024310 (2006)
41. X.-B. Wang, H.-K. Woo, X. Huang, M.M. Kappes, L.-S. Wang, Phys. Rev. Lett. **96**, 143002 (2006)
42. A. Herlert, L. Schweikhard, M. Vogel, Eur. Phys. J. D **16**, 65 (2001)
43. K.J. Taylor, C.L. Pettiette-Hall, O. Cheshnovsky, R.E. Smalley, J. Chem. Phys. **96**, 3319 (1992)
44. M. Manninen, J. Mansikka-aho, H. Nishioka, Y. Takahashi, Z. Phys. D **31**, 259 (1994)
45. L. Schweikhard, S. Krückeberg, K. Lützenkirchen, C. Walther, Eur. Phys. J. D **9**, 15 (1999)
46. H. Weidele, U. Frenzel, T. Leisner, D. Kreisle, Z. Phys. D **20**, 411 (1991)
47. H.-U. Hasse, St. Becker, G. Dietrich, N. Klisch, H.-J. Kluge, M. Lindinger, K. Lützenkirchen, L. Schweikhard, J. Ziegler, Int. J. Mass Spectrom. Ion Process. **132**, 181 (1994)
48. C. Walther, G. Dietrich, M. Lindinger, K. Lützenkirchen, L. Schweikhard, J. Ziegler, Chem. Phys. Lett. **256**, 77 (1996); erratum: Chem. Phys. Lett. **262**, 668 (1996)
49. U. Hild, G. Dietrich, S. Krückeberg, M. Lindinger, K. Lützenkirchen, L. Schweikhard, C. Walther, J. Ziegler, Phys. Rev. A **57**, 2786 (1998)
50. C. Walther, G. Dietrich, W. Dostal, S. Krückeberg, K. Lützenkirchen, L. Schweikhard, Eur. Phys. J. D **9**, 455 (1999)
51. L.S. Brown, G. Gabrielse, Rev. Mod. Phys. **58**, 233 (1986)
52. F.G. Major, V.N. Gheorghe, G. Werth, *Charged Particle Traps* (Springer, Berlin, 2005), pp. 51–84
53. G. Savard, St. Becker, G. Bollen, H.-J. Kluge, R.B. Moore, Th. Otto, L. Schweikhard, H. Stolzenberg, U. Wiess, Phys. Lett. A **158**, 247 (1991)
54. S. Guan, A.G. Marshall, Int. J. Mass Spectrom. Ion Process. **157–158**, 5 (1996)
55. A. Herlert, R. Jertz, J. Alonso Otamendi, A.J. González Martínez, L. Schweikhard, Int. J. Mass Spectrom. **218**, 217 (2002)
56. L. Schweikhard, A.G. Marshall, J. Am. Soc. Mass Spectrom. **4**, 433 (1993)
57. A. Gustafsson, A. Herlert, F. Wenander, Nucl. Instrum. Methods Phys. Res. A **626–627**, 8 (2011)
58. A. Herlert, Ch. Borgmann, D. Fink, Ch. Holm Christensen, M. Kowalska, S. Naimi, Hyperfine Interact. **199**, 231 (2011). doi:10.1007/s10751-011-0316-6
59. L. Schweikhard, K. Hansen, A. Herlert, G. Marx, M. Vogel, Eur. Phys. J. D **24**, 137 (2003)
60. A. Herlert, L. Schweikhard, Int. J. Mass Spectrom. **234**, 161 (2004)
61. A. Herlert, L. Schweikhard, Int. J. Mass Spectrom. **249–250**, 215 (2006)
62. E. Uggerud, P.J. Derrick, J. Phys. Chem. **95**, 1430 (1991)
63. H.J. Cooper, P.J. Derrick, H.D.B. Jenkins, E. Uggerud, J. Phys. Chem. **97**, 5443 (1993)
64. M.F. Jarrold, E.C. Honea, J. Phys. Chem. **95**, 9181 (1991)
65. K. Hansen, A. Herlert, L. Schweikhard, M. Vogel, Int. J. Mass Spectrom. **227**, 87 (2003)
66. Y. Shi, V.A. Spasov, K.M. Ervin, J. Chem. Phys. **111**, 938 (1999)
67. V.A. Spasov, T. Hong Lee, J.P. Maberry, K.M. Ervin, J. Chem. Phys. **110**, 5208 (1999)
68. C. Jackschath, I. Rabin, W. Schulze, Z. Phys. D **22**, 517 (1992)
69. C. Jackschath, I. Rabin, W. Schulze, Ber. Bunsenges. Phys. Chem. **96**, 1200 (1992)
70. W.A. de Heer, Rev. Mod. Phys. **65**, 611 (1993)

71. D. Löffler, J.M. Weber, M.M. Kappes, J. Chem. Phys. **123**, 224308 (2005)
72. B. Concina, M. Neumaier, O. Hampe, M.M. Kappes, Int. J. Mass Spectrom. **252**, 110 (2006)
73. B. Concina, M. Neumaier, O. Hampe, M.M. Kappes, J. Chem. Phys. **128**, 134306 (2008)
74. X.-B. Wang, L.-S. Wang, Annu. Rev. Phys. Chem. **60**, 105 (2009)